Articles

Reversible Dimerization of Acid-Denatured ACBP Controlled by Helix A4[†]

Wolfgang Fieber,[‡] Birthe B. Kragelund,[‡] Morten Meldal,[§] and Flemming M. Poulsen*[,‡]

Department of Protein Chemistry, Institute of Molecular Biology, University of Copenhagen, Øster Farimagsgade 2A, DK-1353 Copenhagen, Denmark, and Department of Chemistry, Carlsberg Laboratory, Gamle Carlsberg Vej 10, DK-2550 Valby, Copenhagen, Denmark

Received August 20, 2004; Revised Manuscript Received November 8, 2004

ABSTRACT: The peptide segment corresponding to helix A4 in acyl-coenzyme-A-binding protein (ACBP) is an exceptionally stable helix in the denatured state of the protein as well as in its isolated form. Circular dichroism spectroscopy showed an α-helix content in the helix A4 peptide (HA4) of 45%, and under denaturing conditions at pH 2.3, helix conformations are still populated in 24% of the ensemble of molecules. The structure of HA4 at atomic resolution was assessed using nuclear magnetic resonance (NMR) spectroscopy. Long-range NOEs between remote residues at opposite peptide ends suggested the formation of an antiparallel homodimer, and the resulting structure was treated as the minimum higher-order structure. The dimerization property of helix A4 is maintained in the full-length protein under denaturing conditions. NMR diffusion studies and concentration-dependent experiments on ACBP at low pH proved the formation of dimers and revealed a cooperative stabilization of helix A4 in this process. This emphasizes its special role in the structure formation in the denatured state of ACBP. No dimers are formed in the presence of guanidine hydrochloride, which underlines the fundamental difference between the nature of these two denatured states.

Structural biology's scope has been extended toward the unfolded state of proteins in the past decade. Many protein domains and full-length proteins display intrinsic properties of local or globular disorder (*1*), and these proteins have been found to be involved in fundamental regulatory cellular processes (*2*). Partially folded or unfolded proteins are prone to aggregation, and their defined role in the formation of amyloid fibrils became a breakthrough in the understanding of the molecular basis of several neurodegenerative diseases such as Alzheimer's, Parkinson's, or Creutzfeld-Jakob disease (*3*). Knowledge about the structural properties of the unfolded state may therefore be one key to a fundamental understanding of these processes. On the other hand, in the protein-folding reaction, the special role of unfolded states is in part implicated by the presence of significant amounts of residual structure (*4*). In particular, the formation of nativelike turns, transient formation of α helices, and hydrophobic clusters have been described (*5*−*9*). These preformations can be the driving forces in the protein-folding initiation process in terms of structural organization, thermodynamics, or kinetics (*10*, *11*). Non-nativelike tertiary interactions have been observed as well, and these supposedly have a guiding effect in these processes (*12*).

Nuclear magnetic resonance (NMR)[1] spectroscopy is the only technique that provides insight into the structure and dynamics of unfolded states of proteins at the atomic level (*13*). In recent years, new experiments have been developed that are of great importance for the understanding of the role of the residual structure in unfolded states for the formation of the native protein. When secondary chemical shifts, scalar coupling, heteronuclear relaxation, and short-range nuclear Overhauser effects (NOEs) are exploited, local secondary structure formation could be observed in several denatured proteins (*5*, *6*, *14*, *15*). Long-range distance restraints from site-directed spin labeling and paramagnetic relaxation enhancement (*16*, *17*), long-range NOEs (*18*), and residual dipolar couplings (*19*−*21*) were additionally found to provide useful information about the structure in denatured proteins.

The major drawback in studying unfolded states of proteins is the structural heterogeneity and conformational averaging as well as the low concentration in the thermodynamic equilibrium with the stable, folded states. This is usually

[†] W.F. is the recipient of an Erwin Schrödinger Fellowship (J2229-B07) from the Austrian Science Foundation (FWF). We also thank the John and Birthe Meyer Foundation for the financial support to the structural biology and NMR laboratory (to F.M.P.). We acknowledge the support of the Carlsberg Foundation (to F.M.P.).

* To whom correspondence should be addressed. Telephone: +45 353 22077. Fax: +45 353 22075. E-mail: fmp@apk.molbio.ku.dk.

[‡] University of Copenhagen.

[§] Carlsberg Laboratory.

[1] Abbreviations: ACBP, acyl-coenzyme-A-binding protein; HA4, helix A4 peptide; GuHCl, guanidine hydrochloride; ANS, 8-anilinonaphthalene-1-sulfonic acid; NMR, nuclear magnetic resonance; NOE, nuclear Overhauser effect; PG-SLED, pulse-gradient-stimulated echo longitudinal encode−decode; HSQC, heteronuclear single-quantum coherence spectroscopy; DQF−COSY, double-quantum-filtered-correlated spectroscopy; TOCSY, total correlation spectroscopy; NOESY, nuclear Overhauser effect spectroscopy; CD, circular dichroism; rt, room temperature.

10.1021/bi0481949 CCC: $30.25
Published on Web 01/11/2005

overcome by destabilizing the protein using heat, chemical denaturants, or acids. However, these methods do not only disrupt the chemical equilibrium of the protein-folding reaction but also may interfere differently with the chemical equilibriums both with respect to the mechanism of folding and to the formation of a residual structure in denatured states (*15*, *22*−*24*).

The present study focuses on the effects of different denaturants on the residual structure in the denatured state of acyl-coenzyme-A-binding protein (ACBP). This 86-residue, single-domain protein folds and unfolds in an apparent two-state mechanism (*25*). In its native state, ACBP is folded into a skewed four-α-helix bundle structure, stabilized by only three identified hydrophobic minicores (*26*). Structure studies of the denatured state of ACBP have shown the presence of both nativelike secondary and tertiary structure (*17*, *21*, *27*, *28*). Although the features are similar in the denatured states at low pH and in the presence of high concentrations of GuHCl, the extent of structure formation is different. The content of transient α-helical structure in segments of native α helices is higher at pH 2.3 than in the presence of 2.5 M guanidine hydrochloride (GuHCl) at pH 5.3 (*21*, *27*, *28*). Magnetization transfer and relaxation studies of the equilibrium between folded and unfolded states (*28*) showed that ACBP folds and unfolds in an apparent two-state reaction in the presence of GuHCl, whereas the data of acid-denatured ACBP could not be fit to such a model, suggesting a major difference between both denatured states.

MATERIALS AND METHODS

Expression and Purification of ACBP. ^{15}N- and ^{13}C,^{15}N-labeled bovine ACBP was expressed and purified as described (*29*).

Synthesis and Purification of Helix A4 Peptide (HA4). HA4 (Ac-GTSKEDAMKAYIDKVEELKKKYGI-NH_2) corresponds to residues 63−86 of ACBP and comprises the fourth α-helix A4 segment of ACBP. It was synthesized on a Synergy Personal Peptide Synthesizer using the standard Fmoc/TBTU-based peptide-coupling procedures in *N*-methyl pyrrolidone for amino acids and a deprotection cycle for 20 min with piperidine. The linker was a Rink Amide linker to provide the peptide amide upon cleavage. Automatic detection of coupling times was derived from preceding deprotection elution profiles at 290 nm. The synthesis did not present any aggregation problems, and cycle times were from 1 to 3 h. The synthesis was completed by acetylation with HOAc/TBTU and deprotection and cleavage with 95% TFA. Filtration and lyophilization gave 84 mg of crude material that was ∼50% pure according to analytical HPLC: 50 min gradient of 0−50% buffer B (0.1% TFA/95% acetonitrile/H_2O) in buffer A (0.1% TFA in 5% acetonitrile/H_2O). Purification by preparative HPLC using the same system and a 1.2 h gradient gave 21 mg of pure peptide. The product was analyzed by analytical HPLC (>98% pure) and amino acid analysis. Further characterization by NMR as described below confirmed the structure.

NMR Spectroscopy. All NMR experiments performed with ACBP were recorded at 298 K on Varian Unity Inova 750 and 800 MHz instruments. The PG-SLED pulse sequence was used to determine the hydrodynamic radius of denatured ACBP (*30*, *31*). Proteins were dissolved in D_2O (99.5%, Cambridge Isotope Laboratories), and the pH was adjusted without correcting for the H/D isotope effect. The observed deuterium isotope effect on pH electrodes (*32*) is counterbalanced by the change in pK_a values of ionizable groups in the protein of equal magnitude but reversed in sign (*33*). Thus, the same ionization state of proteins can be approximated in H_2O and D_2O at the same readings of the glass electrode (*34*). Protein concentrations were determined using far-UV absorbance and varied between 0.4 and 0.5 mM. Stock solutions of GuDCl were prepared by repeatedly dissolving GuHCl in D_2O and freeze-drying the solutions to completely exchange labile hydrogens by deuterons. The final concentration of GuDCl was determined by refractive index (*35*). A series of 25 1D ^{1}H experiments was recorded by increasing the gradient strengths of the en- and decoding pulses from 1 to 46 G cm^{-1}. The diffusion delay was kept constant at 100 ms. The spectra were processed using 1 Hz exponential window functions, and peaks were integrated over the whole aliphatic and aromatic region of the spectrum, respectively, using VNMR software. Dioxane was used as an internal standard with a hydrodynamic radius of 2.12 Å (*30*). Decay rates for both the protein and the internal standard were obtained by fitting the peak integrals to Gaussian functions using gnuplot software (http://gnuplot.info), and the apparent hydrodynamic radius of the protein could directly be obtained (*30*, *31*). As the dioxane signal overlapped with aliphatic signals of the protein, a sum of two Gauss functions, one with a decay rate kept constant at the determined value for the protein, was used to fit the dioxane integrals. The variance of hydrodynamic radii at the same pH value was approximately 0.3 Å.

NMR experiments at equilibrium conditions between folded and unfolded states of ACBP were performed at pH 3.08. The solutions contained 10% D_2O (v/v) and were buffered by 20 mM sodium citrate. To overcome differential relaxation effects, totally relaxed ^{15}N,^{1}H-heteronuclear single-quantum coherence spectroscopy (HSQC) experiments were recorded with a delay of 5 s between the individual scans (*36*). The peaks were fitted to Gaussian profiles in both the *F1* and *F2* dimensions by nonlinear line-shape modeling using nlinLS software (*37*). A standard HNCA spectrum was recorded to determine the C^α chemical-shift values of a 30 μM solution ACBP at pH 2.3 (*38*, *39*). All NMR spectra of ACBP were transformed with nmrPipe software (*37*) and analyzed using NMRView (*40*).

Standard homonuclear double-quantum-filtered-correlated spectroscopy (DQF−COSY), total correlation spectroscopy (TOSCY), and nuclear Overhauser effect spectroscopy (NOESY) spectra of unlabeled HA4 dissolved in 20 mM sodium acetate at pH 5.3 and 10% D_2O (v/v) to a concentration of 3.2 mM were recorded at 298 K on a Bruker 600 MHz spectrometer with mixing times of 45 ms (TOCSY) and 80, 150, and 200 ms (NOESY). All spectra were transformed using the MNMR software, and assignments and data management were done using PRONTO^{3D} software (*41*). $^3J_{H^N H^\alpha}$ coupling constants were determined as described (*42*). Dilution series of HA4 at pH 5.3, 298 K, were recorded on a Varian 500 MHz spectrometer of samples from 3.2 mM to 32 μM with the number of transients increasing from 4 to 40 000.

Generation of Unfolded Structures. InitTraj, which is part of the TRADES software package (*43*), was used to generate

random-coil structures of ACBP. Parameters were set as described (*44*). A total of 10 000 structures was obtained using the three-state GOR method to account for the residue-specific conformational propensity. The radius of gyration of each structure was calculated using HYDROPRO (*45*). Probability distributions for each experimental hydrodynamic radius were determined according to eq 4b in Choy et al. (*46*) with the single fitting parameter σ obtained from least-squares fitting. Experimental values of hydrodynamic radii were converted into radii of gyration using the linear relationship determined for ACBP (*17*).

Fluorescence Spectroscopy and 8-Anilinonaphthalene-1-sulfonic Acid (ANS) Binding. ANS binding was measured at various pH values at room temperature (rt) by fluorescence spectroscopy using a Perkin−Elmer LS50 B fluorimeter. The [ACBP]/[ANS] ratio was kept constant at 1:50 with a protein concentration of 4 μM. Three accumulated spectra were averaged at each pH with excitation at 385 nm, and emission was measured from 450 to 550 nm with slit widths of 2.5 nm. All samples were unbuffered, and the pH was measured immediately before and after measurements.

Circular Dichroism (CD) Spectroscopy. Far-UV CD spectra of both ACBP and HA4 were recorded on a Jasco 810 spectrapolarimeter at rt. The samples were dissolved in either water adjusted to pH 2.3 or in 20 mM sodium acetate at pH 5.3, and the final concentration was 10 μM (HA4) and 15 μM (ACBP), respectively. Each spectrum is an average of up to six spectra recorded from 250 to 190 nm.

Structure Calculation. The structure of the HA4 dimer was calculated using standard simulated annealing protocols of the XPLOR-NIH 3.8 software (*47*). An initial set of 200 structures was generated and interactively analyzed until a set of more than 50 structures without any distance violations beyond 0.3 Å and no angle violations over 5° was reached. The 20 structures with the lowest potential energy were selected to represent the structure of the HA4 dimer. An overview of experimental constraints and structural statistics is given in Table 1. The final structures were analyzed by PROCHECK NMR (*48*) and visualized by INSIGHTII (MSI).

Table 1: Summary of Restraints and Structural Statistics for the HA4−HA4B Dimer[a]

restraints for calculation (per dimer)	
total NOE restraints	368
intraresidue	74
short range	226
long range	10
intermonomer	58
dihedral angle restraints	20
restraint violations	
NOE violations > 0.3 Å	0
rmsd	0.008 ± 0.002
dihedral violations > 5°	0
rmsd	0.03 ± 0.007
deviation from idealized geometry (rms)	
improper	3.64 ± 0.001
bond	0.008 ± 0.002
angle	1.13 ± 0.001
XPLOR energies (kcal mol^{-1})[b]	
total	1012 ± 2
bond	45.6 ± 0.2
angle	286 ± 0.5
improper	777 ± 0.2
NOE restraints	0.7 ± 0.3
dihedral angle constraints	0.007 ± 0.003
rmsd of atomic positions (Å)	
backbone (residues 67−80)	0.57 ± 0.10
backbone all	1.5 ± 0.4
heavy atoms (residues 67−80)	1.2 ± 0.1
heavy atoms all	1.7 ± 0.3
Ramachandran plot statistics residues 67−80 (%)	
most favored and additionally allowed	98.6
generously allowed	1.5
disallowed	0.0

[a] Structural statistics are calculated for the ensemble of 20 least-violated structures with the lowest energy. [b] The nonbonded energies were calculated using the nonbonded energy function of PROLSQ using the parameter file PARALLHGD5.3.pro (*63*).

RESULTS AND DISCUSSION

Comparison of Hydrodynamic Radii of ACBP in GuHCl and at Low pH. Hydrodynamic radii of ACBP at different denaturing conditions were obtained from pulsed-field-gradient NMR diffusion experiments (PG-SLED) (*30*, *31*). The decay of protein signal intensities was fit to a single Gaussian, and the apparent decay rate is a weighted average of contributions from folded and unfolded molecules. Changes in apparent hydrodynamic radii can thus be used to characterize changes in the relative populations of the two states. ACBP unfolds in a cooperative transition as a function of GuHCl concentration, where the hydrodynamic radius increases from 17.6 Å in the folded state to 25.1 Å in the unfolded state in the presence of 3 M GuHCl (Figure 1a). In a recent study, this value has been found to correspond excellently to the radius calculated over an ensemble of structures of ACBP at 3 M GuHCl, which was obtained from a combination of experimental spin-label relaxation data and restrained computer simulations (*17*). The experimental hydrodynamic radius of folded ACBP is very close to the calculated value of 18.1 Å from the solution structure of ACBP (PDB entry 1NTI) using HYDROPRO (*45*). Upon further addition of GuHCl, the radius increases linearly up to a value of 26.2 Å at 5 M. The initial decrease in apparent radius between 0 and 1 M GuHCl in the denaturation curve is due to a slight aggregation of the native protein, which is disturbed in the presence of low denaturant concentrations.

Acid denaturation of ACBP also leads to a significant increase in the hydrodynamic radius compared to the native state. A cooperative transition between folded and unfolded states is observed between pH 3.6 and 2.5 with a transition midpoint at ca. pH 3.0 (Figure 1b). The apparent hydrodynamic radius of ACBP reaches its maximum at pH 2.3 with a value of 29.4 Å, where the protein is fully unfolded with respect to the denaturation curve (*28*). Below pH 2.3, the hydrodynamic radius of ACBP decreases again and reaches a value of 26.0 Å at pH 1.35. Electrostatic repulsion of positive charges is supposed to be the major driving force for protein denaturation at low pH values (*4*). However, high concentrations of conjugated bases present at low pH values can reduce the charge repulsion by binding to the positively charged sites, which leads to a more compact structure of the denatured protein (*49*). This mechanism probably causes the reduction in hydrodynamic radii of ACBP at very low pH values. In fact, an increase in α-helical content by lowering the pH value could be determined by CD spectroscopy, and the ellipticity at 222 nm was −4700 deg cm^2 dmol^{-1} at pH 2.2 and −7400 deg cm^2 dmol^{-1} at pH 0.67.

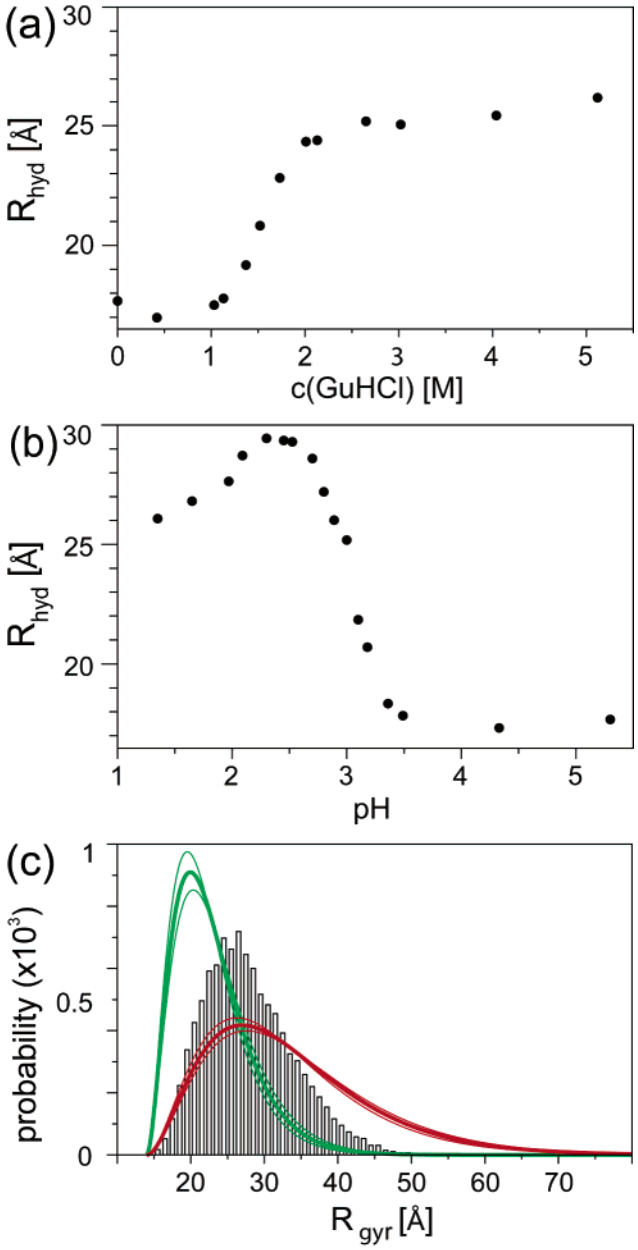

FIGURE 1: Hydrodynamic radius of ACBP (a) as a function of the GuHCl concentration and (b) as a function of pH. (c) Histogram of the distribution of values of radii of gyration in a random-coil ensemble of ACBP comprising 10 000 structures generated with TRADES (*43*). Thick lines represent the calculated radius of gyration probability distribution functions (*46*) for experimental, ensemble-averaged hydrodynamic radius values of 25.1 Å (3 M GuHCl, green) and 29.4 Å (pH 2.3, red), respectively. Thin lines resemble the experimental error of the hydrodynamic radii of 0.3 Å.

The apparent radius of 29.4 Å at pH 2.3 is about 4 Å larger than the corresponding state at 3 M GuHCl, where more than 99% of the molecules are unfolded (*28*). To illustrate this difference, size distribution curves have been calculated for ensembles of structures with overall hydrodynamic radii of 25.1 and 29.4 Å, respectively (Figure 1c). These are compared to the size distribution of random-coil structures of ACBP generated by TRADES (*43*). ACBP at 3 M GuHCl clearly contains a higher number of compact molecules than the random-coil state, suggesting the presence of long-range interactions (*17*). In contrast, the determined probability distribution function that corresponds to the experimental size

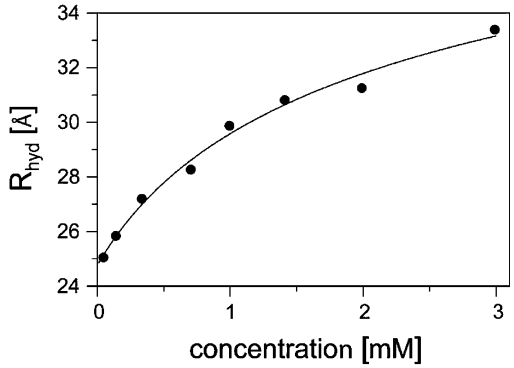

FIGURE 2: Hydrodynamic radius of ACBP at pH 2.3 as a function of the protein concentration. The line represents the fit of the data according to a two-state association reaction between mono- and dimeric unfolded states. See the text for the fitting parameters.

of acid-denatured ACBP suggests an ensemble of structures that is even more unfolded than the random-coil state. Previous studies of ACBP have shown that the amount of secondary structure is significantly higher in the acid-denatured state than that in the GuHCl-denatured state, and thus, the ensemble of acid-denatured ACBP was expected to be even more compact (*27*, *28*).

Protein Concentration Dependence of the Hydrodynamic Radius at pH 2.3. To examine this further, the possibility of aggregation or oligomerization of ACBP at pH 2.3 was tested by measuring the hydrodynamic radius as a function of the protein concentration (Figure 2). A decrease of the hydrodynamic radius of the protein occurs upon dilution of the sample. The apparent radius decreases from 33.4 Å at a protein concentration of 3 mM to 25.1 Å at 50 μM. This is a good indication for the presence of multimeric forms of the unfolded protein molecules at pH 2.3. The concentration dependence of the hydrodynamic radius was fitted to a monomer/dimer equilibrium model. The parameters in this two-state model are the hydrodynamic radii of mono- and dimeric unfolded states, R_M and R_D, and the equilibrium association constant K_a, respectively (Figure 2). The respective fitting results are 24.8 $\pm$ 0.3 Å for R_M, 44.6 $\pm$ 3.1 Å for R_D, and 212 $\pm$ 153 M^{-1} for K_a. This suggests that the monomeric state at low pH is similar in size to the GuHCl-denatured state. The dimer interaction is weak according to the obtained equilibrium association constant K_a. The ability of ACBP to form a weak dimer at low pH seems to be an intrinsic property of the unfolded state because the formation occurs concomitantly with the increase in the fraction of unfolded molecules in the denaturation curve. At pH values below 2.3, the acid-induced compaction of ACBP leads to a decrease in the apparent hydrodynamic radius. However, the measured radius is still concentration-dependent, indicating the presence of dimeric states at these pH values, too. The formation of ACBP dimers in the presence of GuHCl at pH 5.3 has not been observed. The protein concentration dependence of the hydrodynamic radii is not compatible with a bimolecular equilibrium and indicates nonspecific aggregation at higher protein concentrations in the presence of GuHCl.

In a previous work (*28*), transition midpoints of pH denaturation curves showed significant concentration dependence, and we determined values at pH 2.92 at 10 μM (CD spectroscopy) and at pH 3.12 at 1 mM (NMR spectroscopy).

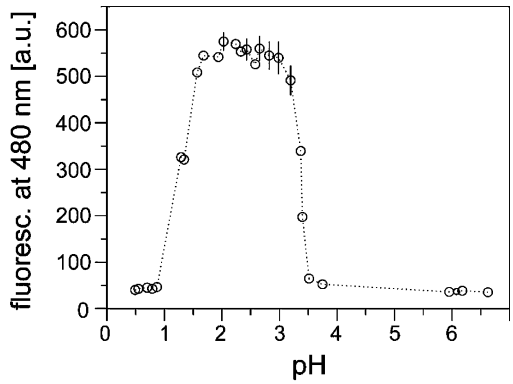

FIGURE 3: Fluorescence emission intensity of ANS at 480 nm (excitation at 385 nm) at rt in the presence of ACBP as a function of pH. The ratio of [ANS]/[ACBP] was 50:1 with a protein concentration of 4 μM.

In contrast, GuHCl denaturation curves did not show any concentration dependence and were identical using fluorescence and CD and NMR spectroscopy, respectively. Consequently, the effect of the protein concentration on the denaturation curves of ACBP was tested and showed transitions midpoints at pH 2.86 $\pm$ 0.02 (1.7 μM) and 2.97 $\pm$ 0.01 (167 μM), respectively, determined by CD spectroscopy. This agrees with the assumption of a three-state model of acid-denatured ACBP, where the monomer/dimer equilibrium of the unfolded state is shifted toward dimer formation at higher protein concentrations, while shifting the folding/unfolding equilibrium toward the unfolded state.

The results presented above also enlighten previous observations from magnetization transfer and relaxation studies applied at equilibrium conditions of ACBP at pH 3.08 and in the presence of 1.6 M GuHCl, respectively (*28*). In contrast to the GuHCl-denatured state, a two-state model was not sufficient to yield good fitting results for the data of the acid-denatured state. Instead, the time evolution of auto and exchange peaks could be fit by anticipating a simplified model including a second unfolded subpopulation that contributes to the observed peak intensities only through relaxation but not through chemical exchange. It is shown here that the acid-denatured state of ACBP is in fact a three-state equilibrium and that mono- and dimeric unfolded states are in fast exchange on the NMR time scale (see below). A re-evaluation of the magnetization transfer study based on such equilibrium is not possible because both unfolded states cannot be discriminated in the NMR spectra leaving the system underdetermined. Nevertheless, we suppose that the results of this study actually originate from the presence of a three-state equilibrium, where the decay of auto and exchange peaks are driven by a complicated interplay of the chemical exchange rates between folded and unfolded and mono- and dimeric states of ACBP, respectively.

ANS Binding of Acid-Denatured ACBP. To determine the nature of the interface that plays a role in the dimerization process, the binding affinity of ACBP to ANS has been tested. ANS is a fluorescent hydrophobic probe and has been widely used as an indicator for molten globule structures of proteins (*50*). When the pH of the solution of ACBP is lowered, ANS binding increases sharply between pH 3.5 and 3 and reaches a plateau value between pH 3 and 1.5 (Figure 3). This happens concomitantly with the unfolding of the protein as shown by the CD titration curve (*28*). It illustrates the extensive presence of hydrophobic patches and suggests that the observed dimerization reaction is mediated by hydrophobic binding of two ACBP molecules. It has to be pointed out that at protein concentrations used in ANS-binding studies unfolded ACBP is practically entirely in the monomeric form. ACBP at pH 2.3 is not considered to be a molten globule, though. It was demonstrated that the secondary structure of proteins in the molten globule state is close to that in the native state (*51*). This is definitely not the case for acid-denatured ACBP (*28*). When the pH of the solution is lowered further, the ANS fluorescence signal intensity at pH 1 drops to the value at neutral pH. Whether this effect originates only from compaction of the protein and the resulting reduced exposed hydrophobic surface area amenable to ANS binding or if ANS also has a reduced hydrophobic affinity at such low pH values is not known.

Effect of Protein Concentration on Chemical Equilibria and ^{15}N Relaxation. The overall equilibrium of acid-denatured ACBP has further been tested for its concentration dependence at the transition midpoint of denaturation at pH 3.08 (*28*). ^{15}N,^{1}H-HSQC spectra were recorded under fully relaxed conditions (*36*), and slow exchange on the NMR time scale allows for the separate analysis of the unfolded and folded states. The ratios of peak integrals of residues in the two states, referred to as the apparent equilibrium constant, K_{app}, have been determined at protein concentrations of 2.2 mM and 45 μM, respectively. It has to be noted that K_{app} comprises both consecutive equilibria between folded and unfolded and mono- and dimeric states, respectively, because the latter are in fast chemical exchange on the NMR time scale and are not discriminated in the spectrum. Because peak integrals are dependent on the relaxation rates of the individual residues and are highly sequence-dependent in the unfolded form, K_{app} does not represent the correct ratio of folded and unfolded states in terms of concentration. Instead, it is regarded to be an operational, descriptive parameter.

Looking at the K_{app} values of ACBP at 2.2 mM, a sequence-specific pattern displaying segments of different values can be recognized (Figure 4a). At a low protein concentration (45 μM), all residues, apart from residues in helix A4, show reduced K_{app} values compared to the measurement at 2.2 mM. This indicates either a change in the equilibrium distribution of unfolded and folded molecules or differential relaxation properties of the unfolded states. The ^{15}N line widths in the unfolded states of ACBP at both concentrations show nearly identical values along the protein backbone from residues 2 to 65 (Figure 4b), indicating very similar relaxation processes. The observed shift in K_{app} is therefore likely due to an actual change in the population of native and unfolded conformers, with an increase in the unfolded form at higher protein concentration because of the concentration-dependent protein dimerization reaction. This is compatible with the results from CD spectroscopy denaturation curves at different protein concentrations.

The second remarkable difference between measurements at 45 μM and 2.2 mM is the lower dispersion of K_{app} values along the protein backbone (Figure 4a). The effect is mainly due to the fact that K_{app} values in the segment of helix A4 increase upon dilution, which is the opposite behavior for all of the other residues. The outstanding properties of helix A4 can be illustrated by the differential line widths of the $N\text{-}H^N$ signals of the unfolded state in the ^{15}N,^{1}H-HSQC

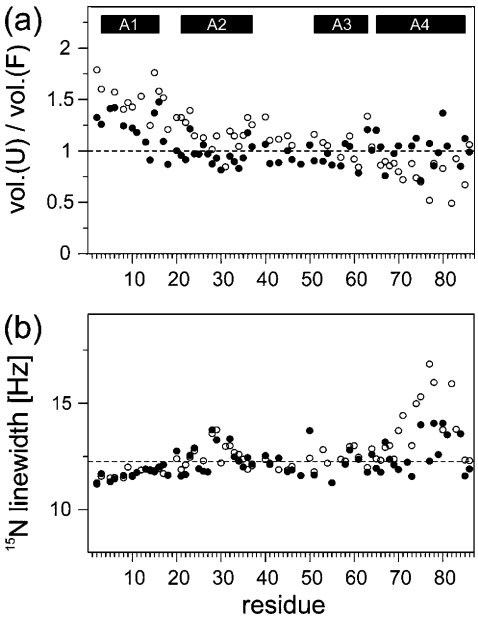

FIGURE 4: Comparison of properties of ACBP under equilibrium conditions at pH 3.08. Data were recorded at 2.2 mM (○) and 45 μM (●). (a) Volume ratio (K_{app}) of unfolded and folded peaks obtained from ^{15}N,^{1}H-HSQC spectra. The black bars denote the location of the four helices in the native state of ACBP. The dashed line at $K_{app} = 1$ is used to guide the eye. (b) ^{15}N line widths of the unfolded state of ACBP. The dashed line represents the average line width of 12.2 Hz for ACBP at 45 μM.

spectra at the two protein concentrations (Figure 4b). The signals experience significantly higher line-broadening effects at 2.2 mM, and the resulting lower peak intensities are reflected by lower values of K_{app}. It indicates the presence of substantial conformational exchange in the region of helix A4 in the milli- to microsecond time scale. Similar line-broadening effects as a consequence of an association reaction have been observed for the isolated helix H of apomyoglobin (*52*). It is therefore also likely that the effects in helix A4 of ACBP originate from transient structure formation in the dimerization reaction, demonstrating the exquisite role of this segment.

Apart from the large differences in helix A4, the profiles of ^{15}N line widths of the unfolded state of ACBP are similar at 2.2 mM and 45 μM. In detail, the line widths are higher than the average in helices A2 and A4. This is in accordance with previous observations of nativelike interactions in the denatured state between helices A2 and A4 and the concomitant restriction because of the formation of the transient α-helical structure (*21*).

Effect of Protein Concentration on C$^{\alpha}$ Chemical Shifts. C$^{\alpha}$ chemical shifts were used to monitor residue-specific structural changes as a function of the protein concentration. An HNCA spectrum was recorded at 30 μM, and the extracted chemical shifts were compared to those from a 1 mM sample (*28*) (Figure 5). Two regions can be identified, which display higher than average chemical-shift differences. These correspond to the positions of the native helices A2 and A4. In helix A4, the C$^{\alpha}$ chemical shifts decrease up to 0.4 ppm with dilution, whereas in helix A2, the maximum chemical-shift change upon dilution is 0.2 ppm. Residues located in other protein segments do not show significant chemical-shift differences. These results show that the amount of transient α-helical structures at pH 2.3 increases

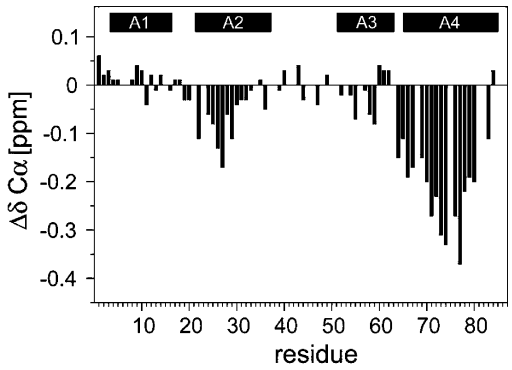

FIGURE 5: C$^{\alpha}$ chemical-shift difference of ACBP between samples at 30 μM and 1 mM (30 μM−1 mM). The black bars denote the location of the four helices in the native state of ACBP.

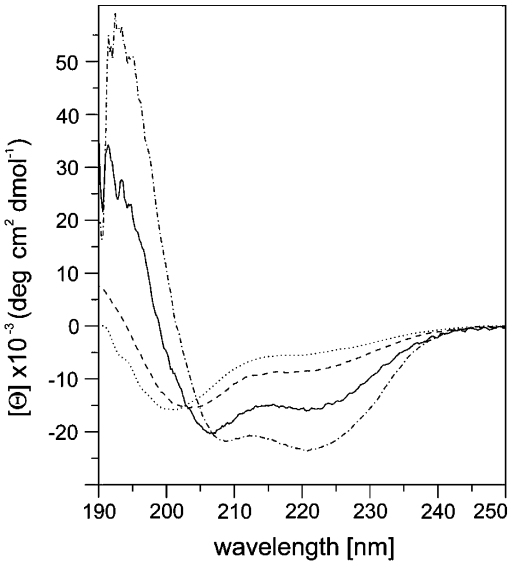

FIGURE 6: Far-UV CD spectra of ACBP (···) and HA4 (- - -) in water at pH 2.3 and of ACBP (-·-) and HA4 (—) in 20 mM sodium acetate at pH 5.3.

in segments A2 and A4 at higher protein concentrations (*53*), suggesting a cooperative stabilization of the segment upon dimerization. The apparent chemical-shift changes for residues in helix A2 is likely to be a consequence of the observed nativelike interactions between helices A2 and A4 (*21*). However, at this point it cannot be ruled out, whether the increase in helical content in helix A2 upon concentrating the sample is a passive effect, where the helix formation is enhanced by the presence of a more stable template of helix A4, or an active effect in that also residues in helix A2 form part of the hydrophobic interface mediating the dimerization reaction.

Isolated Helix A4 Forms Stable Structures of Higher Order. To dissect the contribution of helix A4 to the stability and dimerization properties of full-length ACBP, a peptide fragment that comprises only helix A4 was synthesized (HA4) and analyzed using CD and NMR spectroscopy. The CD spectrum of HA4 displays the typical features of an α helix with two minima at 208 and 222 nm (Figure 6), and the calculated α-helical content is 45% at rt by comparing the mean residue ellipticity at 222 nm to a reference base spectrum from eight proteins (*54*). The intensity ratio of the absorption bands at 222 and 208 nm ($\theta_{222}/\theta_{208}$) of 0.81 indicates that at a peptide concentration of 10 μM HA4 exists

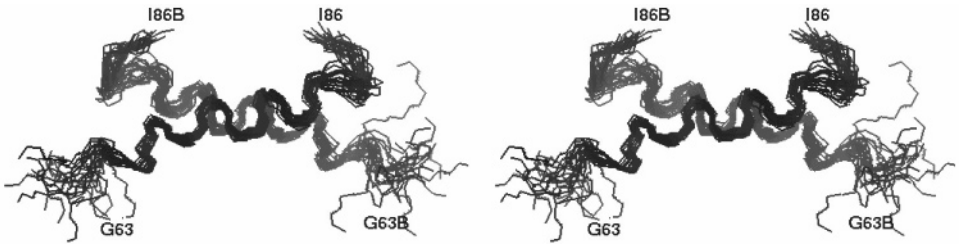

FIGURE 7: Stereoview of the ensemble of the 20 lowest energy structures of the dimeric structure of HA4. The root-mean-square deviation (rmsd) of the backbone atoms in the region [Glu67-Leu80, Glu67B-Leu80B] is 0.57 ± 0.1 Å.

as an isolated helix (*55*). The amount of residual structure is therefore quite exceptional. A high α-helical content is also retained under acidic conditions at pH 2.3, where helix conformations are still populated by 24% of the ensemble of molecules.

The structure of HA4 at atomic resolution was assessed using NMR spectroscopy. Initially, several unambiguous long-range NOEs between $Y73_{HA4}$ and $Y84_{HA4}$ were observed indicating either a highly bent structure of the peptide or the presence of higher-order structures. Dilution of the NMR sample from 3.2 mM to 32 μM resulted in the collapse of chemical-shift dispersion strongly indicating the generation of concentration-dependent structure formation. The final set of NOEs contained the expected short and medium range contacts typical for stable α helices as well as additional long-range NOEs corresponding to contacts between residues from the N and the C termini of HA4. To accomplish for these long-range NOEs, a minimum higher-order structure of HA4 was anticipated by the formation of an antiparallel homodimer, with the N terminus of one unit being close to the C terminus of the other unit. From initial structure calculations using the observed typical α-helix contacts and the unambiguous long-range NOEs, more interpeptide NOEs were iteratively assigned and used in subsequent calculations. Only one set of signals is observed for HA4, indicating a symmetric environment of the protons. Because of this inherent symmetry of the system, assignments and verification of NOEs in the central interface were complicated and for $Val77_{HA4}-Val77_{HA4B}$ obviously not possible. The structure of the symmetric antiparallel homodimer of HA4 is shown in Figure 7. It was calculated based on 368 NOE restraints and 20 dihedral angle restraints, distributed as shown in Table 1. No violations beyond 0.3 Å were seen. In another calculation protocol anticipating a monomeric, highly bent peptide, several violations of the final NOE set were observed, which disfavor the presence of such a conformation.

Because all NMR experiments of HA4 have been conducted at high peptide concentration (3.2 mM), the possibility of structure formation of a higher order than that of a dimer cannot be disregarded (*52*). As a result of the antiparallel assembly of the two HA4 monomers, the formation of a trimeric structure (*56*) can be ruled out, because any orientation of the third helix would result in asymmetry. The formation of a symmetric tetramer of HA4, instead, would be compatible with the chemical-shift data. However, the assignment of NOEs in terms of a tetramer is difficult to accomplish, because intra- and interhelical contacts between two parallel-situated helices could no longer be discriminated. Moreover, inter-NOEs to residues of the two antiparallel helices would have to be treated as degenerated, and subsequent assignment to a single NOE or weighing of a degenerate NOE would require *a priori* knowledge of the dimeric structure.

The interhelical NOEs involve mainly side chains of residues Ala72, Tyr73, Leu80, Tyr84, and Ile86. Val77 is situated in the center of the HA4 sequence and also participates in hydrophobic interactions, but because of the symmetry, the NOEs are left unassigned. The resulting structure has almost exclusively hydrophobic side chains forming the interface between the two HA4 units, whereas charged amino acids point away and are solvated by water molecules. The hydrophobic interface can be dissected into three segments. The first segment constitutes a mini core and comprises the side chains of Ala69, Ala72, and Tyr73 of one HA4 unit and the hydrophobic part of Lys76, Leu80, and Tyr84 of the second HA4 unit, respectively. This minicore is mirror-imaged at the other end of the dimeric structure. The third hydrophobic segment is at the center of the HA4 dimer and encompasses Val77 of both units, which form additional van der Waals contacts to the hydrophobic part of the side chains of Lys81 and Tyr73. The helical axes of the two monomeric units are slightly bent toward each other similar to the structure of a coiled coil.

In the structure of ACBP, hydrophobic residues of helix A4 form interactions to residues of both helix A2 and helix A1 (*26*). The hydrophobic residues in helix A4 form a contiguous stretch, which covers about one-half of the side of the helix. In the structure of the HA4 dimer, part of this broad hydrophobic stripe does not get completely buried but is exposed to the solvent to a certain amount, causing two distinguishable sides of the structure. Whereas charged residues mainly occupy the first side, the second side exposes a number of hydrophobic side chains to the solvent, involving Tyr73, Ile74, and Val77. The hydrophobic, solvent-exposed side in the structure of the dimer would thus provide a potential additional interaction surface. The dimeric structure of HA4 is in full compliance with the final NOE set and must be recognized as the minimal structural unit assessed by the peptide.

Comparison of the HA4 Dimer to the Structure of ACBP. The hydrophobic dimer interface of the HA4 monomers is equivalent to the interaction site between helices A4 and A2 in the structure of folded ACBP (Figure 8). The crossing of the two HA4 helices is analogous to the crossing of helices A2 and A4 in ACBP and very different to the interface of helices A1 and A4 (parts a and b of Figure 8). The dimer interface involves in particular residues Ala69, Tyr73, Leu80, and part of Val77. In native-folded ACBP, these residues are involved in interactions with Ile27 in helix A2. These are also part of a nativelike folding transition-state interaction (*21*). The five residues are conserved class 1 (highly con-

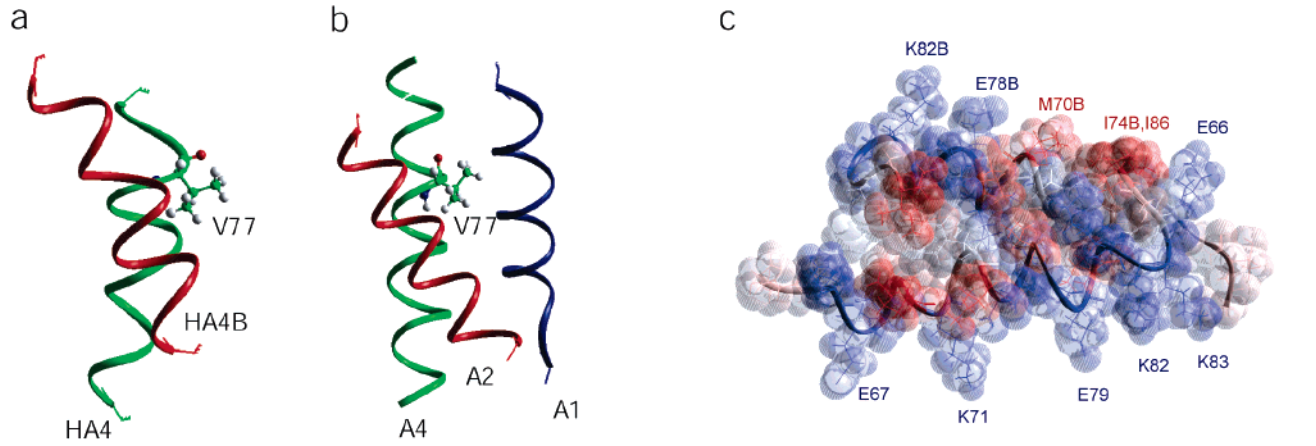

FIGURE 8: Structure of the HA4 dimer. (a) Helix−helix crossing of the HA4 dimer, with Val77 shown as a ball-and-stick model. Only residues from Glu67-Leu80 (green) and Glu67B-Leu80B (red) are shown as a smooth ribbon. (b) Helix−helix crossing and orientation in bovine ACBP of the helices A1 (blue, Ser1-Leu15), A2 (red, Asp21-Val36), and A4 (green, Ser65-Tyr84) shown as a smooth ribbon. Val77 is shown as a ball-and-stick model. (c) Surface of the HA4−HA4B dimer colored according to hydrophobicity with polar residues in blue and hydrophobic residues in red. Tyrosine residues are colored gray. The available hydrophobic patch formed by residues Met70, Ile74, and Ile86 is indicated.

served) or class 2 (conserved as hydrophobic residues) residues in all known isoforms of ACBP (*57*), indicating a key role in structure stabilization of both the native of the unfolded state and of the transition-state structures (*58*). Side chains of amino acids, which are involved in binding to helix A1 in native ACBP, are more or less exposed to the solvent in the HA4 dimer. These are Val77, Met70, and Ile74 (Figure 8c).

In principle, the hydrophobic dimerization interface of two helix A4 segments in acid-denatured ACBP could be represented by the sides of helix A4, which either interact with helix A1 or with helix A2 in the native state, respectively, or by a mixture of both of them. The interface toward helix A2 seems to be more favorable because it also appears in the HA4 dimer. However, because of nativelike, cooperatively stabilized interactions between helices A2 and A4 (*21*), this site is occupied in a certain amount of protein conformations. The observation in the present study that helical structure in segments A2 and A4 is additionally stabilized as a function of the protein concentration and thus as a function of dimer formation does not support the A2−A4 interface as the binding site in the dimer. On the other hand, it is known from earlier studies that helix A1 in the unfolded state is remote from helices A2 and A4 and seems to undergo nearly unrestricted segmental motion (*17*, *27*). Consequently, the exposure of hydrophobic side chains in helix A4 to the solvent by the release of helix A1 from the stable, native hydrophobic core opens a new possible interaction surface. It is therefore conceivable that the A1−A4 interface represents another interaction site, where hydrophobic residues in helix A4 mediate homodimerization of ACBP.

Role of Helix A4 in Folded and Unfolded States of ACBP. The segment corresponding to helix A4 in the native state of ACBP shows evidence of having a special role in the stabilization of this protein. It seems to be the predominant structure-forming part in the denatured, transition, and native states of the protein, respectively. Helix A4 is the segment with the highest helix content in the denatured state of ACBP (*27*, *28*) and is involved in nativelike interactions with helix A2 at both acidic conditions and in the presence of GuHCl (*17*, *21*). In the folding process of ACBP, conserved hydrophobic residues in helices A1, A2, and A4 form a nativelike structure, which has been shown to be the rate-limiting step for the reaction (*58*). Finally, helix A4 is strongly involved in the stabilization of the native structure of ACBP through hydrophobic interactions to residues in helix A1 and A2 (*26*). This exceptional role is similar to that of helix H of apomyoglobin, which also participates in the structure of the denatured state (*15*), the intermediate state of the folding process (*5*, *59*), and the native state (*60*), respectively. However, the amount of residual structure in the denatured state is significantly higher in helix A4 of ACBP (*28*) than that in helix H (*15*). This can also be illustrated by the comparison of the helical content of the isolated peptide segments helix H (30% at 0 °C) (*52*) and HA4 (45% at rt), presented in this work.

The high secondary structure content in helix A4 is already manifested in its calculated helix propensity, which is twice as high as the helix propensity of helix H of apomyoglobin under identical conditions and three times higher than that of the other three helical segments in ACBP (*61*, *62*). It is plausible that this preformed helical structure in solution acts as a well-ordered template that facilitates recognition of other parts of the protein and thus is the nucleus for intramolecular interactions. This can be revealed by the observed nativelike interactions to helix A2 in the denatured state. Likewise, the formation of the rate-limiting structure between helices A1, A2, and A4 is likely to be governed by the template properties of helix A4. Whereas the structure between A2 and A4 is already established in the denatured state, helix A1 does not strongly interact with the rest of the protein (*17*, *27*). Not until the residue-specific interactions between helices A1 and A4 are formed (*58*) is the protein able to proceed the folding path towards the native state. The observed dimerization reaction mediated by helix A4 is, although non-native, yet another example of the template function of helix A4. The arrangement of hydrophobic residues into a specific pattern can easily be recognized by a second helix A4 segment, and the binding results in a cooperative stabilization of the structure.

CONCLUSIONS

The present study shows the existence of non-native interactions in the acid-denatured state of ACBP. The interactions are mediated by the segment corresponding to helix A4 in the native state, and they describe a cooperative association of two denatured ACBP molecules to a homodimer. No dimerization reaction is observed for the denatured state of ACBP in the presence of GuHCl. This emphasizes that care must be taken when denatured states of proteins under different denaturing conditions are compared. The results support and enlighten a previous study of ACBP, where experimental results were not compatible with a two-state equilibrium between folded and unfolded forms of ACBP at low pH (*28*). It is suggested here that the three-state equilibrium involving the dimer accounts for the observed effects.

The present results furthermore identify helix A4 as the prime structural element in ACBP, which acts to stabilize the denatured form according to two different mechanisms. In contrast to the nativelike interactions with helix A2 (*17*, *21*), the homodimerization reaction is clearly a non-native interaction that occurs at higher protein concentrations. However, both interactions seem to occur simultaneously, which is accomplished by the hydrophobic nature of helix A4, and it underlines the central importance of this protein segment in ACBP.

ACKNOWLEDGMENT

We thank Kaare Teilum and Jens Kaalby Thomsen for many useful discussions.

SUPPORTING INFORMATION AVAILABLE

Figure showing the mean residue ellipticity at 222 nm of ACBP at low pH values determined by CD spectroscopy, figure showing CD denaturation curves of ACBP at different protein concentrations, and figure showing a dilution series of HA4 monitored by NMR spectroscopy. This material is available free of charge via the Internet at http://pubs.acs.org.

REFERENCES

1. Wright, P. E., and Dyson, H. J. (1999) Intrinsically unstructured proteins: Re-assessing the protein structure−function paradigm, *J. Mol. Biol. 293*, 321−331.
2. Romero, P., Obradovic, Z., Kissinger, C. R., Villafranca, J. E., Garner, E., Guilliot, S., and Dunker, A. K. (1998) Thousands of proteins likely to have long disordered regions, *Pac. Symp. Biocomput.* 437−448.
3. Taylor, J. P., Hardy, J., and Fischbeck, K. H. (2002) Toxic proteins in neurodegenerative disease, *Science 296*, 1991−1995.
4. Dill, K. A., and Shortle, D. (1991) Denatured states of proteins, *Annu. Rev. Biochem. 60*, 795−825.
5. Eliezer, D., Yao, J., Dyson, H. J., and Wright, P. E. (1998) Structural and dynamic characterization of partially folded states of apomyoglobin and implications for protein folding, *Nat. Struct. Biol. 5*, 148−155.
6. Brutscher, B., Bruschweiler, R., and Ernst, R. R. (1997) Backbone dynamics and structural characterization of the partially folded A state of ubiquitin by ^{1}H, ^{13}C, and ^{15}N nuclear magnetic resonance spectroscopy, *Biochemistry 36*, 13043−13053.
7. Yi, Q., Scalley-Kim, M. L., Alm, E. J., and Baker, D. (2000) NMR characterization of residual structure in the denatured state of protein L, *J. Mol. Biol. 299*, 1341−1351.
8. Wong, K. B., Freund, S. M., and Fersht, A. R. (1996) Cold denaturation of barstar: ^{1}H, ^{15}N, and ^{13}C NMR assignment and characterisation of residual structure, *J. Mol. Biol. 259*, 805−818.
9. Fieber, W., Schneider, M. L., Matt, T., Kräutler, B., Konrat, R., and Bister, K. (2001) Structure, function, and dynamics of the dimerization and DNA-binding domain of oncogenic transcription factor v-Myc, *J. Mol. Biol. 307*, 1395−1410.
10. Myers, J. K., and Oas, T. G. (2001) Preorganized secondary structure as an important determinant of fast protein folding, *Nat. Struct. Biol. 8*, 552−558.
11. Chiti, F., Taddei, N., Webster, P., Hamada, D., Fiaschi, T., Ramponi, G., and Dobson, C. M. (1999) Acceleration of the folding of acylphosphatase by stabilization of local secondary structure, *Nat. Struct. Biol. 6*, 380−387.
12. Klein-Seetharaman, J., Oikawa, M., Grimshaw, S. B., Wirmer, J., Duchardt, E., Ueda, T., Imoto, T., Smith, L. J., Dobson, C. M., and Schwalbe, H. (2002) Long-range interactions within a nonnative protein, *Science 295*, 1719−1722.
13. Dyson, H. J., and Wright, P. E. (1998) Equilibrium NMR studies of unfolded and partially folded proteins, *Nat. Struct. Biol. 5*, 499−503.
14. Alexandrescu, A. T., and Shortle, D. (1994) Backbone dynamics of a highly disordered 131 residue fragment of staphylococcal nuclease, *J. Mol. Biol. 242*, 527−546.
15. Yao, J., Chung, J., Eliezer, D., Wright, P. E., and Dyson, H. J. (2001) NMR structural and dynamic characterization of the acid-unfolded state of apomyoglobin provides insights into the early events in protein folding, *Biochemistry 40*, 3561−3571.
16. Gillespie, J. R., and Shortle, D. (1997) Characterization of long-range structure in the denatured state of staphylococcal nuclease. I. Paramagnetic relaxation enhancement by nitroxide spin labels, *J. Mol. Biol. 268*, 158−169.
17. Lindorff-Larsen, K., Kristjansdottir, S., Teilum, K., Fieber, W., Dobson, C. M., Poulsen, F. M., and Vendruscolo, M. (2004) Determination of an ensemble of structures representing the denatured state of ACBP, *J. Am. Chem. Soc. 126*, 3291−3299.
18. Mok, Y. K., Kay, C. M., Kay, L. E., and Forman-Kay, J. (1999) NOE data demonstrating a compact unfolded state for an SH3 domain under non-denaturing conditions, *J. Mol. Biol. 289*, 619−638.
19. Shortle, D., and Ackerman, M. S. (2001) Persistence of native-like topology in a denatured protein in 8 M urea, *Science 293*, 487−489.
20. Ackerman, M. S., and Shortle, D. (2002) Robustness of the long-range structure in denatured staphylococcal nuclease to changes in amino acid sequence, *Biochemistry 41*, 13791−13797.
21. Fieber, W., Kristjansdottir, S., and Poulsen, F. M. (2004) Short-range, long-range, and transition state interactions in the denatured state of ACBP from residual dipolar couplings, *J. Mol. Biol. 339*, 1191−1199.
22. Dubey, V. K., and Jagannadham, M. V. (2003) Differences in the unfolding of procerain induced by pH, guanidine hydrochloride, urea, and temperature, *Biochemistry 42*, 12287−12297.
23. Schwarzinger, S., Wright, P. E., and Dyson, H. J. (2002) Molecular hinges in protein folding: The urea-denatured state of apomyoglobin, *Biochemistry 41*, 12681−12686.
24. Buck, M., Radford, S. E., and Dobson, C. M. (1993) A partially folded state of hen egg white lysozyme in trifluoroethanol: Structural characterization and implications for protein folding, *Biochemistry 32*, 669−678.
25. Kragelund, B. B., Robinson, C. V., Knudsen, J., Dobson, C. M., and Poulsen, F. M. (1995) Folding of a four-helix bundle: Studies of acyl-coenzyme A binding protein, *Biochemistry 34*, 7217−7224.
26. Andersen, K. V., and Poulsen, F. M. (1993) The three-dimensional structure of acyl-coenzyme A binding protein from bovine liver: Structural refinement using heteronuclear multidimensional NMR spectroscopy, *J. Biomol. NMR 3*, 271−284.
27. Teilum, K., Kragelund, B. B., and Poulsen, F. M. (2002) Transient structure formation in unfolded acyl-coenzyme A-binding protein observed by site-directed spin labelling, *J. Mol. Biol. 324*, 349−357.
28. Thomsen, J. K., Kragelund, B. B., Teilum, K., Knudsen, J., and Poulsen, F. M. (2002) Transient intermediary states with high and low folding probabilities in the apparent two-state folding equilibrium of ACBP at low pH, *J. Mol. Biol. 318*, 805−814.
29. Mandrup, S., Hojrup, P., Kristiansen, K., and Knudsen, J. (1991) Gene synthesis, expression in *Escherichia coli*, purification, and characterization of the recombinant bovine acyl-CoA-binding protein, *Biochem. J. 276*, 817−823.

30. Jones, J. A., Wilkins, D. K., Smith, L. J., and Dobson, C. M. (1997) Characterisation of protein unfolding by NMR diffusion measurements, *J. Biomol. NMR 10*, 199−203.
31. Wilkins, D. K., Grimshaw, S. B., Receveur, V., Dobson, C. M., Jones, J. A., and Smith, L. J. (1999) Hydrodynamic radii of native and denatured proteins measured by pulse field gradient NMR techniques, *Biochemistry 38*, 16424−16431.
32. Glasoe, P. K., and Long, F. A. (1960) Use of glass electrodes to measure acidities in deuterium oxide, *J. Phys. Chem. 64*, 188−190.
33. Bundi, A., and Wüthrich, K. (1979) ^{1}H NMR parameters of the common amino acid residues measured in aqueous solutions of the linear tetrapeptides H-Gly-Gly-X-L-Ala-OH, *Biopolymers 18*, 285−297.
34. Makhatadze, G. I., Clore, G. M., and Gronenborn, A. M. (1995) Solvent isotope effect and protein stability, *Nat. Struct. Biol. 2*, 852−855.
35. Nozaki, Y. (1972) The preparation of guanidine hydrochloride, *Methods Enzymol. 26*, 43−50.
36. Farrow, N. A., Zhang, O., Forman-Kay, J. D., and Kay, L. E. (1994) A heteronuclear correlation experiment for simultaneous determination of ^{15}N longitudinal decay and chemical exchange rates of systems in slow equilibrium, *J. Biomol. NMR 4*, 727−734.
37. Delaglio, F., Grzesiek, S., Vuister, G. W., Zhu, G., Pfeifer, J., and Bax, A. (1995) NMRPipe: A multidimensional spectral processing system based on UNIX pipes, *J. Biomol. NMR 6*, 277−293.
38. Ikura, M., Kay, L. E., and Bax, A. (1990) A novel approach for sequential assignment of ^{1}H, ^{13}C, and ^{15}N spectra of proteins: Heteronuclear triple-resonance three-dimensional NMR spectroscopy. Application to calmodulin, *Biochemistry 29*, 4659−4667.
39. Grzesiek, S., and Bax, A. (1992) Improved 3D triple-resonance NMR techniques applied to a 31 kDa protein, *J. Magn. Reson. 96*, 432−440.
40. Johnson, B. A., and Blevins, R. A. (1994) NMRVIEW: A computer program for the visualization and analysis of NMR data, *J. Biomol. NMR 4*, 603−614.
41. Kjaer, M., Andersen, K. V., and Poulsen, F. M. (1994) Automated and semiautomated analysis of homo- and heteronuclear multidimensional nuclear magnetic resonance spectra of proteins: The program Pronto, *Methods Enzymol. 239*, 288−307.
42. Ludvigsen, S., Andersen, K. V., and Poulsen, F. M. (1991) Accurate measurements of coupling constants from two-dimensional nuclear magnetic resonance spectra of proteins and determination of φ angles, *J. Mol. Biol. 217*, 731−736.
43. Feldman, H. J., and Hogue, C. W. (2000) A fast method to sample real protein conformational space, *Proteins 39*, 112−131.
44. Choy, W. Y., and Forman-Kay, J. D. (2001) Calculation of ensembles of structures representing the unfolded state of an SH3 domain, *J. Mol. Biol. 308*, 1011−1032.
45. Garcia de la Torre, J., Huertas, M. L., and Carrasco, B. (2000) Calculation of hydrodynamic properties of globular proteins from their atomic-level structure, *Biophys. J. 78*, 719−730.
46. Choy, W. Y., Mulder, F. A., Crowhurst, K. A., Muhandiram, D. R., Millett, I. S., Doniach, S., Forman-Kay, J. D., and Kay, L. E. (2002) Distribution of molecular size within an unfolded state ensemble using small-angle X-ray scattering and pulse field gradient NMR techniques, *J. Mol. Biol. 316*, 101−112.
47. Brunger, A. T. (1992) *Xplor*, manual version 3.0.
48. Laskowski, R. A., Rullmannn, J. A., MacArthur, M. W., Kaptein, R., and Thornton, J. M. (1996) AQUA and PROCHECK-NMR: Programs for checking the quality of protein structures solved by NMR, *J. Biomol. NMR 8*, 477−486.
49. Goto, Y., Takahashi, N., and Fink, A. L. (1990) Mechanism of acid-induced folding of proteins, *Biochemistry 29*, 3480−3488.
50. Ptitsyn, O. B. (1992) in *Protein Folding* (T. E. Creighton, T. E., Ed.) pp 243−300, W. H. Freeman and Company, New York.
51. Vassilenko, K. S., and Uversky, V. N. (2002) Native-like secondary structure of molten globules, *Biochim. Biophys. Acta 1594*, 168−177.
52. Waltho, J. P., Feher, V. A., Merutka, G., Dyson, H. J., and Wright, P. E. (1993) Peptide models of protein folding initiation sites. 1. Secondary structure formation by peptides corresponding to the G- and H-helices of myoglobin, *Biochemistry 32*, 6337−6347.
53. Spera, S., and Bax, A. (1991) Empirical correlation between protein backbone conformation and Cα and Cβ ^{13}C nuclear magnetic resonance chemical shifts, *J. Am. Chem. Soc. 113*, 5490−5492.
54. Chen, Y.-H., Yang, J. T., and Chau, K. H. (1974) Determination of the helix and β form of proteins in aqueous solution by circular dichroism, *Biochemistry 13*, 3350−3359.
55. Cooper, T. M., and Woody, R. W. (1990) The effect of conformation on the CD of interacting helices: A theoretical study of tropomyosin, *Biopolymers 30*, 657−676.
56. Dames, S. A., Kammerer, R. A., Wiltscheck, R., Engel, J., and Alexandrescu, A. T. (1998) NMR structure of a parallel homotrimeric coiled coil, *Nat. Struct. Biol. 5*, 687−691.
57. Kragelund, B. B., Knudsen, J., and Poulsen, F. M. (1999) Acyl-coenzyme A binding protein (ACBP), *Biochim. Biophys. Acta 1441*, 150−161.
58. Kragelund, B. B., Osmark, P., Neergaard, T. B., Schiodt, J., Kristiansen, K., Knudsen, J., and Poulsen, F. M. (1999) The formation of a native-like structure containing eight conserved hydrophobic residues is rate limiting in two-state protein folding of ACBP, *Nat. Struct. Biol. 6*, 594−601.
59. Hughson, F. M., Wright, P. E., and Baldwin, R. L. (1990) Structural characterization of a partly folded apomyoglobin intermediate, *Science 249*, 1544−1548.
60. Kuriyan, J., Wilz, S., Karplus, M., and Petsko, G. A. (1986) X-ray structure and refinement of carbon-monoxy(Fe^{II})-myoglobin at 1.5 Å resolution, *J. Mol. Biol. 192*, 133−154.
61. Munoz, V., and Serrano, L. (1995) Elucidating the folding problem of helical peptides using empirical parameters. III. Temperature and pH dependence, *J. Mol. Biol. 245*, 297−308.
62. Munoz, V., and Serrano, L. (1995) Elucidating the folding problem of helical peptides using empirical parameters. II. Helix macrodipole effects and rational modification of the helical content of natural peptides, *J. Mol. Biol. 245*, 275−296.
63. Linge, J. P., and Nilges, M. (1999) Influence of non-bonded parameters on the quality of NMR structures: A new force field for NMR structure calculation, *J. Biomol. NMR 13*, 51−59.

BI0481949